

Electronic supplementary information

Enhancing internal electric field by Zn²⁺ doping for promoting bulk-charge separation and improving visible photocatalytic activity of Bi₂YO₄Cl

Yuehong Peng ^{a,b}, Jincai Peng ^{a,c}, Liang Xu ^a, Kai Lin ^a, Qi Wang ^{*a}, Zhaoyi Yin ^a,
Jin Han ^a, Jianbei Qiu ^a, Zhengwen Yang ^a, Zhiguo Song ^a, Yongjin Li ^{*a}

^a School of Materials Science and Engineering, Kunming University of Science and Technology, Kunming, 650093, China

^b School of Physics and Electronical Science, Chuxiong Normal University, Chuxiong, 675000, China

^c Dean's Office, Sichuan University of Arts and Science, Dazhou 635000, China

* Corresponding authors.

E-mail addresses: qiwang@kust.edu.cn (Q. Wang), liyongjin@kust.edu.cn (Y. Li).

Experimental

Synthesis

A series of Bi₂YO₄Cl (BY) samples doped with different Zn²⁺ concentrations (4, 6, and 8 mol%) were prepared by a high-temperature solid-state reaction method. NH₄Cl (99.5%, Shanghai, China), Bi₂O₃ (99.99%, Shanghai, China), Y₂O₃ (99.99%, Shanghai, China), and ZnO (99%, Shanghai, China) were used directly without any further purification. And BiOCl was prepared by a solid-state reaction method as

described elsewhere¹. The stoichiometric raw materials were thoroughly mixed by using ethanol as solvent in an agate mortar. After that, the well-mixed powders were calcined at 800 °C for 12 h in a resistance furnace at 5 °C/min rate. After calcinations, the obtained samples were cooled naturally to room temperature and then were ground again into fine powders.

For comparison, the pure BY sample was also synthesized by a similar procedure without adding the ZnO into the mixed powders at the initial stage. The pure BY and Zn²⁺-doped BY with different Zn²⁺ concentrations (4, 6, and 8 mol%) denote as BY, BY-Zn1, BY-Zn2, BY-Zn3, respectively.

Characterization

The crystalline structures of the samples was determined by powder X-ray diffraction (XRD) (Bruker D8 Advance diffractomete with Cu K α radiation(λ =15.406 nm) operating at 40 kV and 30 mA). The morphology of the obtained samples was investigated by using a field emission scanning electron microscopy (FESEM, Hitachi SU-8010) accompanied with energy dispersive spectroscopy (EDS) to examine the chemical composition. The ultraviolet-visible (UV-Vis) diffuse reflectance (DR) spectra were measured by using a Hitachi UV-4100 spectrophotometer equipped with an integrating sphere, and the BaSO₄ was as a reference sample. The X-ray photoelectron spectroscopy spectrum (XPS, Thermo Fisher Scientific ESCALAB 250) was carried out to analyze the surface elemental composition. The surface potentials of the samples were measured by Bruker Dimension Icon atomic force microscope (AFM) in Kelvin probe mode. The zeta

potential of samples was determined by Malvern Zetasizer Nano ZS90 zeta potential analyzer. The photocurrents were measured using an electrochemical workstation (Bio-Logic SP-300) with a standard three-electrode system with a Pt wire as the counter electrode, saturated Hg/Hg₂Cl₂ (in saturated KCl) as the reference electrode, and Na₂SO₄ (0.5 M) aqueous solution as the electrolyte. Xenon lamp (power 500W) was utilized as the light source. The transient photocurrent responses with time (I–t curve) of the working electrodes were measured at a bias potential of 1.5 V during repeated on/off illumination cycles under continuous irradiation. The surface photovoltages (SPV) spectroscopic measurement was carried out based on the lock-in amplifier. It is composed of a monochromatic light source which provided by the 500 W xenon lamp (CHFXM-500 W, Global Xenon Lamp Power) and a monochromator (Omni-5007, Zolix), a lock-in amplifier (SR830-DSP) with a light chopper (SR540), a photovoltage cell and a computer. The femtosecond-resolved transient absorption (TA) spectra were conducted using a HELIOS Fire spectrometer (Ultrafast Systems). The intermediates of TC photodegradation were analyzed by LC/TOF-MS (Agilent 1100 HPLC/TOF) and the total organic carbon (TOC) was measured by Elementar Vario TOC analyzer. The BET surface areas were measured by N₂ adsorption/desorption at 77 K on a micromeritics ASAP-2020 instrument. The EPR (electron paramagnetic resonance) spectra were recorded on an Electron Paramagnetic Resonance (Bruker A300).

Photocatalytic activity experiment

The photocatalytic activities of the as-synthesized samples were evaluated by the

degradation of tetracycline hydrochloride (TCH). A 500 W Xe lamp (CEL-LAX500, Beijing Zhongjiao Jinyuan Technology Co. LTD., China) was adopted as UV-Vis-NIR light source, and a 420 nm cut-off filter was used as a Visible light source (> 420 nm). In each experiment, a certain amount of as-prepared catalyst (50 mg for UV-Vis-NIR photocatalysis and 100 mg for Vis-NIR photocatalysis) was suspended into a 50 mL TCH aqueous solution (10 mg/L) for 60 min vigorously stirring to ensure the establishment of adsorption–desorption equilibrium under dark environment. During the illumination process, about 3 mL of suspension was regularly withdrawn and centrifuged to remove the catalysts particles. The concentration of filtrates was analyzed by measuring the photoabsorption intensity at wavelength of 357 nm for TCH using a Hitachi UV-4100 spectrophotometer.

In addition, active species trapping experiments were carried out by adding different kinds of active species scavengers into the TCH aqueous solution to investigate the reactive species responsible for photocatalytic degradation of TCH. Ascorbic acid, EDTA-2Na, and isopropanol were chosen as $\bullet\text{O}_2^-$, h^+ , and $\bullet\text{OH}$ scavengers, respectively.

Toxicity assessment of the degradation products of TCH

The *E. coli* is selected to evaluate the toxicity of the degradation products of TCH.

Cultivation of *E. coli*: on the ultra-clean platform, 0.1 ml of *E. coli* (ATCC25922) suspension was added into 50 mL of LB and incubated for 14 h at 37 °C in an incubator shaker under 120 r/min to obtain *E. coli* suspension I. Then 0.1 mL of the *E. coli* suspension I was added into another 50 mL of LB and incubated for 24 h under

the same conditions to obtain the *E. coli* suspension II.

3 mL of TCH solution, photocatalysis degradation products of TCH, and normal saline as the control were added to the test tubes, respectively. Subsequently, 1 mL of LB and 1 mL of *E. coli* suspension II were added into the tubes. Then, it was incubated for 24 h at 37 °C in an incubator shaker under 120 r/min. During this period, a certain amount of the *E. coli* suspension was taken out at different incubation times, and the absorbance of *E. coli* was measured at 600 nm using a microplate reader (BIO-RADiMark) to reveal the growth of *E. coli*. The values for growth inhibition I were calculated using the following formula

$$I = (1 - OD_{control}/OD) \times 100\% \quad (1)$$

Where $OD_{control}$ represents the absorbance of the *E. coli* suspension with TCH. Moreover, 100 μ L of the *E. coli* suspension was taken at 8 hours of incubation, and the viable bacteria were counted by the method of 10 times dilution.

Theoretical calculations

In this work, the density functional (DFT) theory calculations were performed with the plane-wave techniques as implemented in the Vienna ab initio simulation package (VASP). The generalized gradient approximation (GGA) in the form of the Perdew-Burke-Ernzerhof (PBE) was applied to describe the electron exchange and correlation energy. And pure and Zn^{2+} -doped BY structures were modeled as a $2 \times 2 \times 2$ super-cell. To model the BY crystal structure with different Zn^{2+} doping modes, Zn^{2+} ions exist in the supercell by occupying Bi^{3+} and Y^{3+} sites, interstitial sites, and lattice interlayers, respectively. We performed Brillouin-zone integrations using Monkhorst-

Pack scheme K-points grid with $(2 \times 2 \times 3)$ mesh for the structure optimization. And an energy cutoff of 520 eV was used for expanding the Kohn-Sham wave functions. All of the structures were relaxed with a conjugate-gradient algorithm until the energy on the atoms less than 1.0×10^{-5} eV. For surface models, a vacuum space larger than 15 Å was inserted in the z direction to prevent the artificial interaction between periodically repeated images.

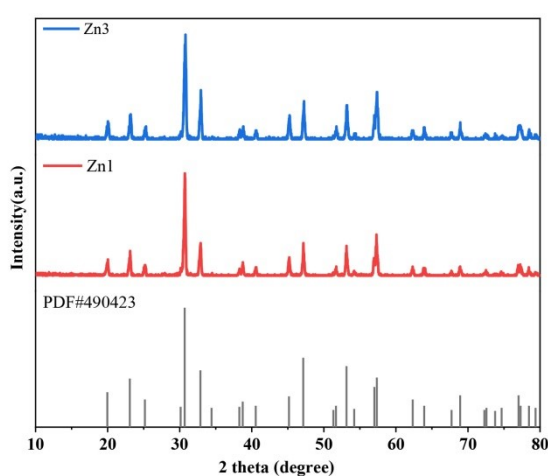


Fig. S1 XRD patterns of the BY-Zn1 and BY-Zn3 samples.

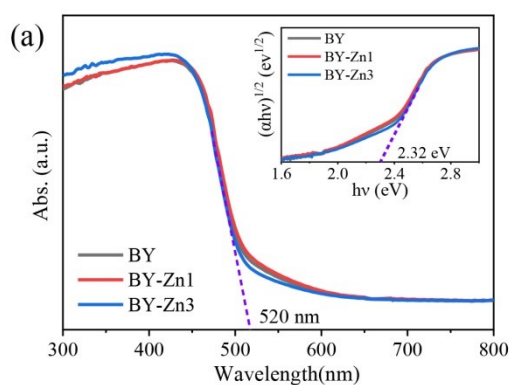


Fig. S2 The UV-Vis DR spectra of the pure BY, BY-Zn1 and BY-Zn3, the inset is the corresponding Tauc plots.

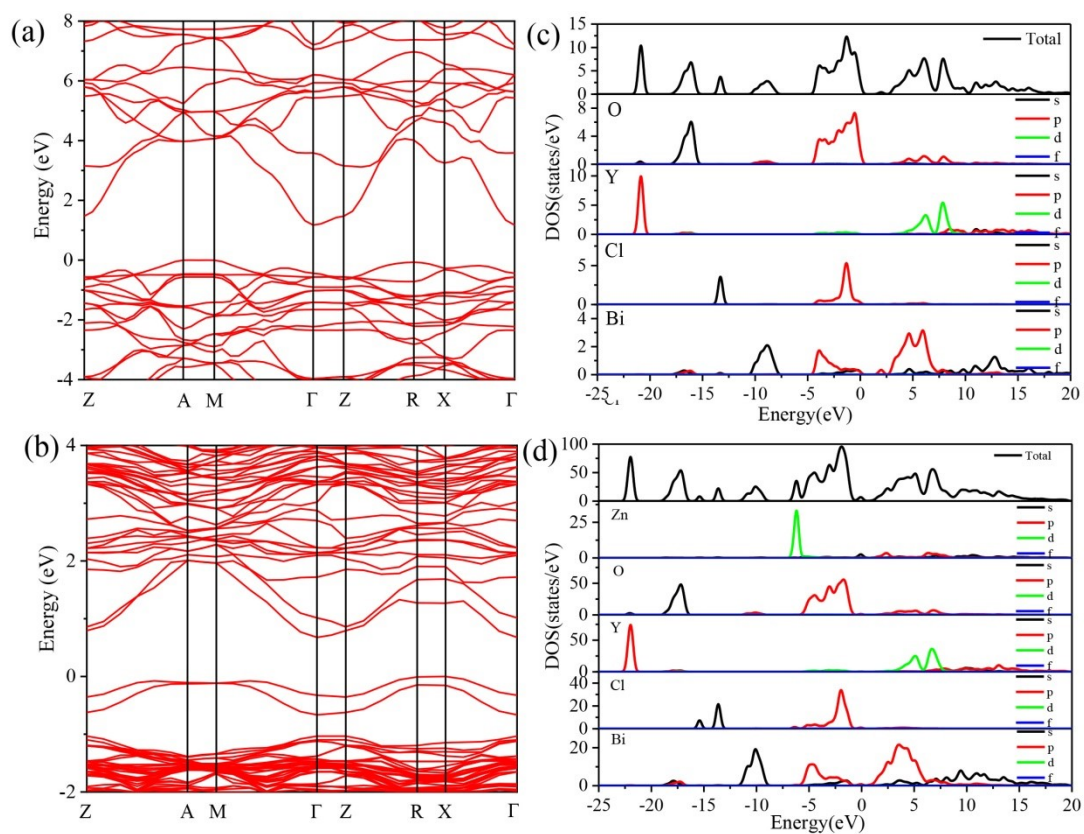


Fig. S3 Band structures and density of states of pure BY (a, c) and Zn-doped BY (b, d).

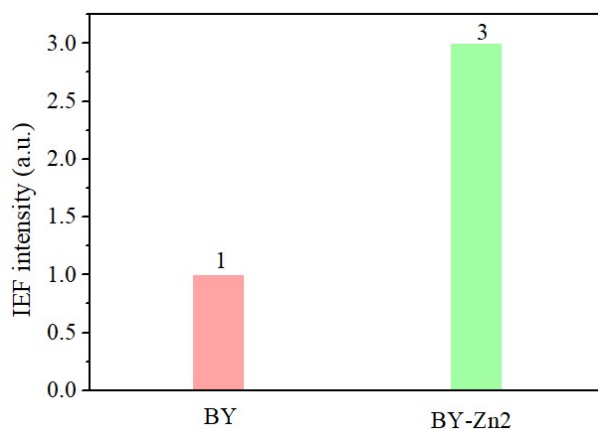


Fig. S4 The IEF intensity of BY and BY-Zn2 samples (assuming the IEF intensity of BY to be “1”).

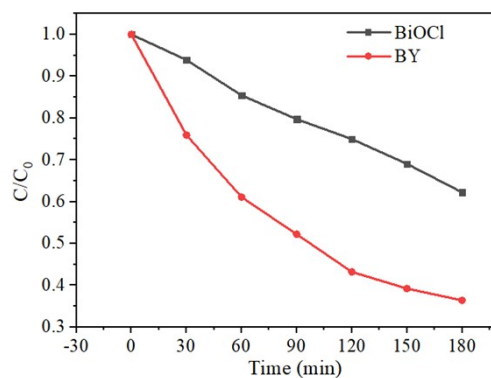


Fig. S5 Photodegradation of TCH over BiOCl and BY under visible light (> 420 nm) irradiation.

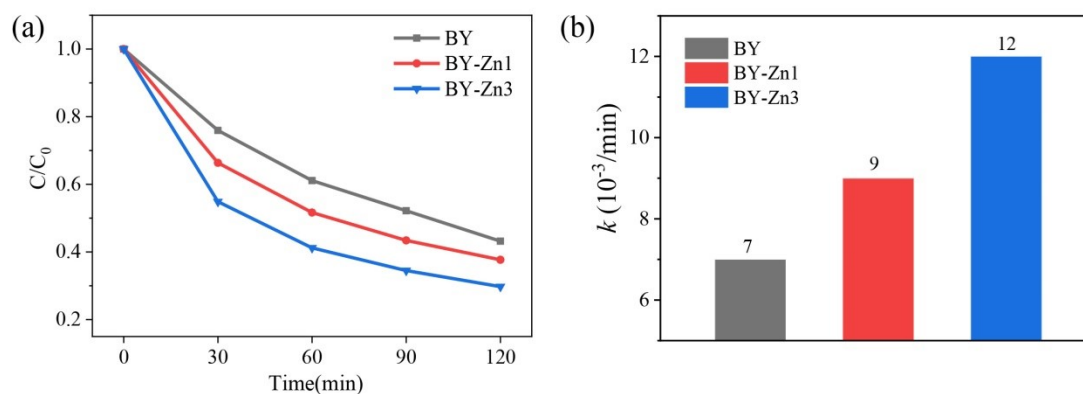


Fig. S6 (a) Photodegradation of TCH over pure BY, BY-Zn1, and BY-Zn3 under visible light (> 420 nm) irradiation; (b) the determined apparent rate constants by pseudo first-order kinetic fitting.

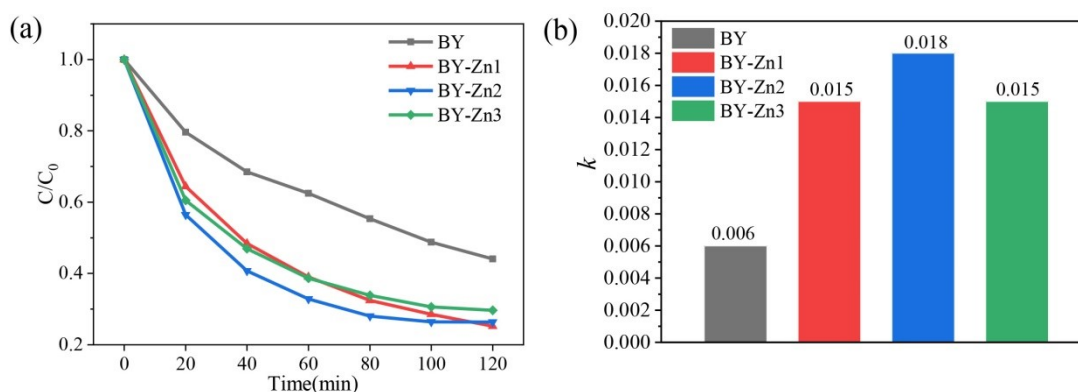


Fig. S7 (a) Photodegradation of TCH over pure BY, BY-Zn1, and BY-Zn3 under UV-Vis light irradiation; (b) the determined apparent rate constants by pseudo first-order kinetic fitting.

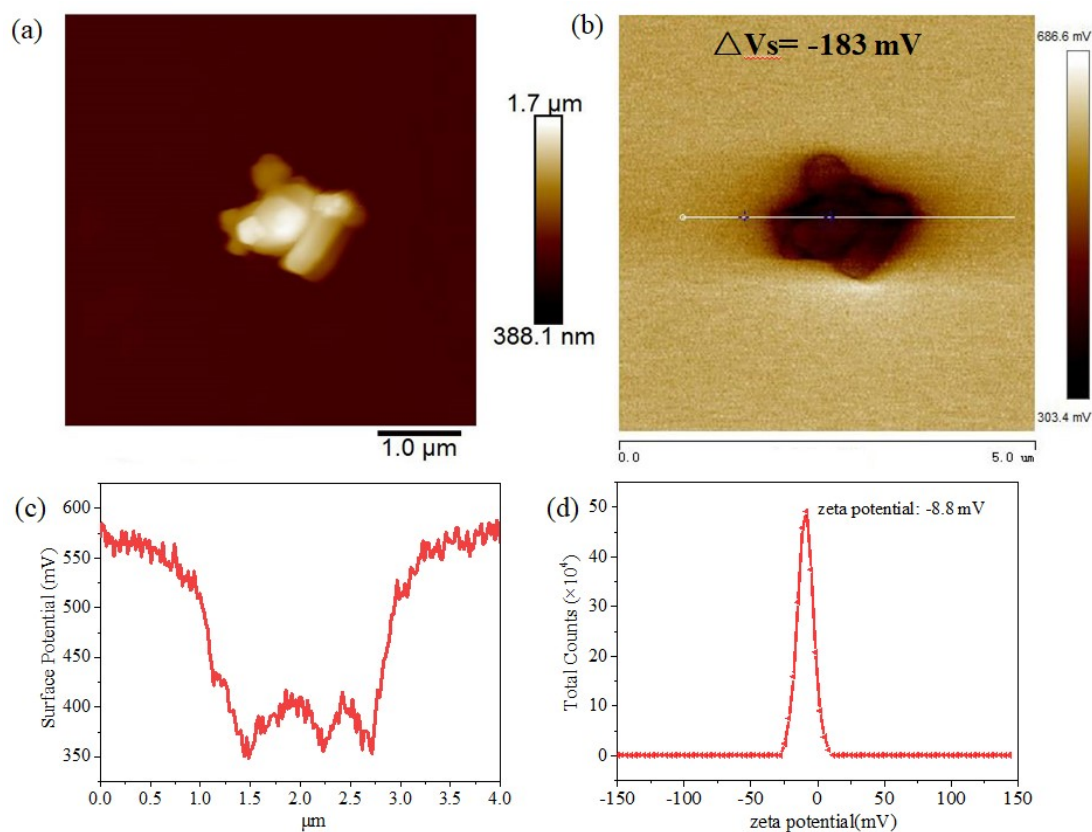


Fig. S8 (a) AFM photos and (b) the surface potential for BY-Zn2 sample after photocatalytic reaction; (c) surface potential profiles along the white lines in Fig. S8b; (d) the zeta potentials of the BY-Zn2 sample after photocatalytic reaction.

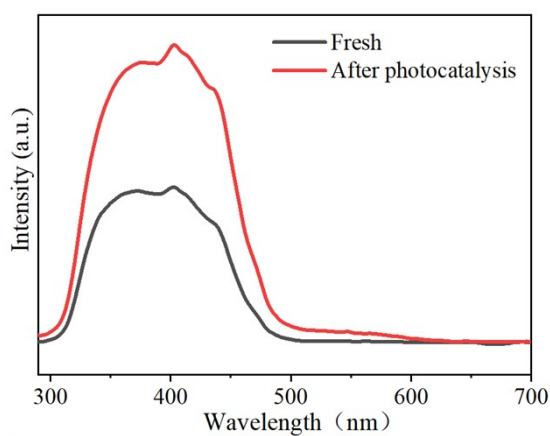


Fig. S9 SPV spectra of the BY-Zn2 sample before and after photocatalytic reaction.

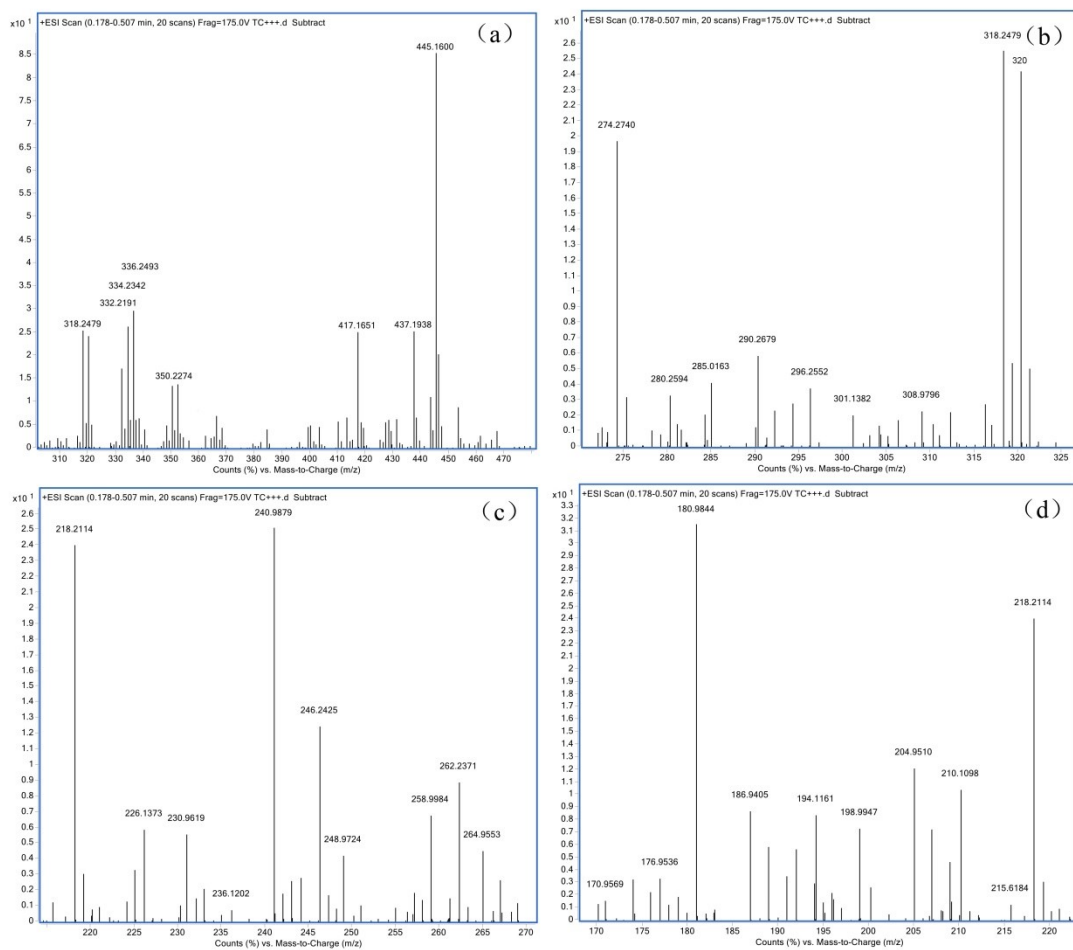
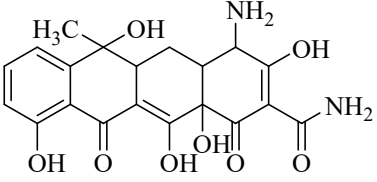
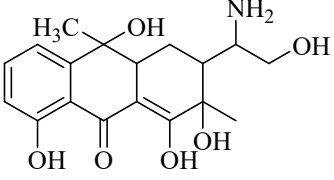
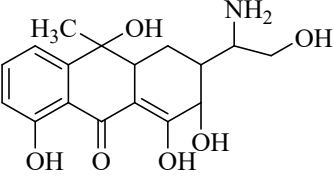
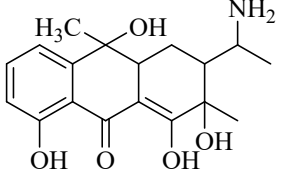
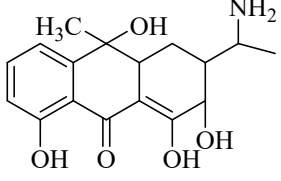
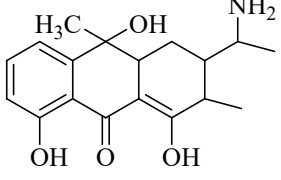
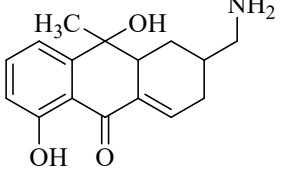
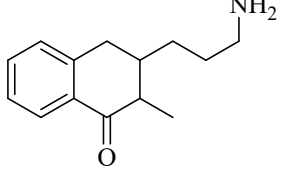
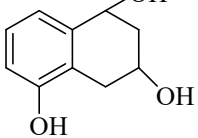


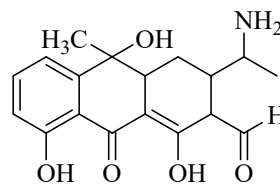
Fig. S10 The Mass spectra of degradation intermediates of TCH.

Table S1 Possible intermediates for degradation of TCH by BY-Zn2 under visible-light irradiation.

Product	m/z	Potential products
Tetracycline	445	

P1	417	
P2	350	
P3	336	
P4	334	
P5	320	
P6	318	
P7	274	
P8	218	
P9	181	

P10 332



P11 241

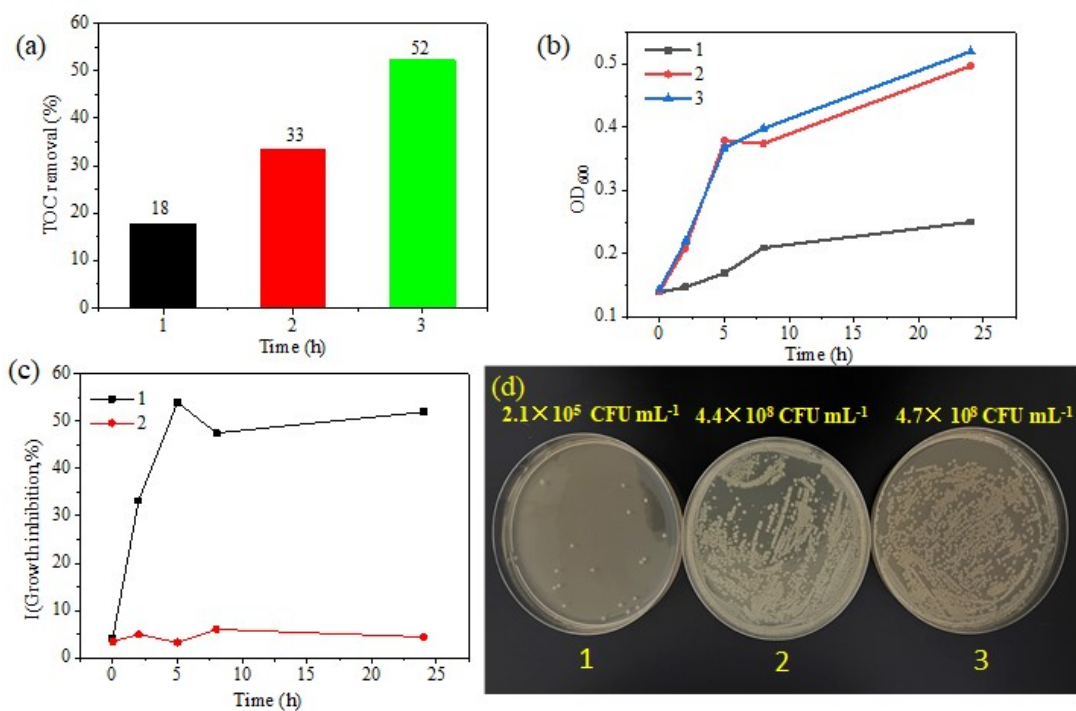
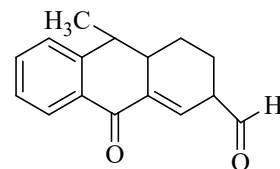


Fig. S11 (a) TOC removal rates of TCH over BY-Zn2 samples; (b) the growth trend, growth inhibition rates and colony formation of *E. coli* in different liquid culture mediums: (1) TCH, (2) the degradation products of TCH, (3) the control group.

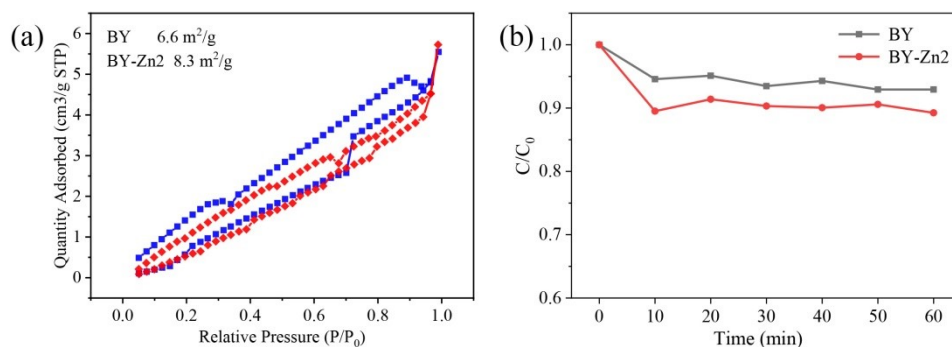


Fig. S12 (a) N₂ adsorption-desorption isotherms for the BY and BY-Zn₂ samples; (b) the adsorption of TCH over BY and BY-Zn₂ in the dark.

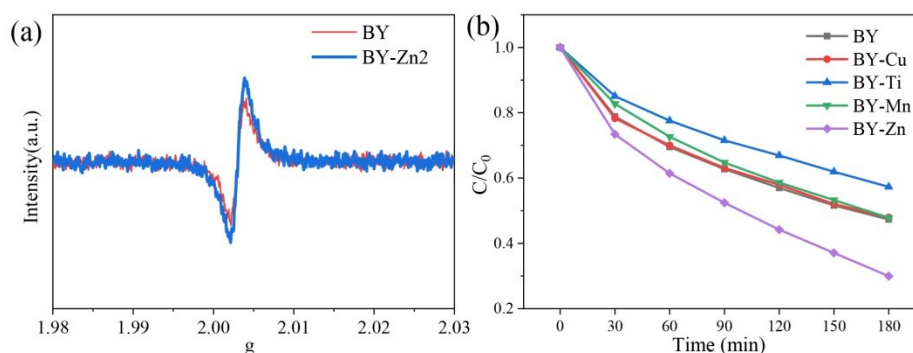


Fig. S13 (a) The EPR spectra for BY and BY-Zn₂; (b) the effect of different transition metal ions doping on photocatalytic activity of BY.

Reference

1. Y. Li, Z. Song, R. Wan, Q. Liu, Y. Zhou, J. Qiu, Z. Yang and Z. Yin, Multi-band photon avalanche controlling performance of BiOCl:Er³⁺ crystals through facile Yb³⁺ doping, *J. M. Chem. C*, 2015, **3**, 8559-8565.